AGU PUBLICATIONS

Water Resources Research

RESEARCH ARTICLE

10.1002/2013WR014834

# A stochastic model of streamflow for urbanized basins

**Alfonso Mejía[1], Edoardo Daly[2], Florian Rossel[1], Tijana Jovanovic[1], and Jorge Gironás[3,4,5]**

[1]Department of Civil and Environmental Engineering, Pennsylvania State University, University Park, Pennsylvania, USA, [2]Monash Water for Liveability, Department of Civil Engineering, Monash University, Clayton, Victoria, Australia, [3]Departamento de Ingeniería Hidráulica y Ambiental, Pontificia Universidad Católica de Chile, Santiago, Chile, [4]Centro de Desarrollo Urbano Sustentable CONICYT/FONDAP/15110020, Santiago, Chile, [5]Centro Interdisciplinario de Cambio Global UC, Pontificia Universidad Católica de Chile, Santiago, Chile

**Key Points:**
- Stochastic model of streamflow in urban basins reproduces flow duration curves
- Link between rainfall and urbanization used to obtain ecohydrological indices
- Long-term transformation of green to blue water important in urban basins

**Correspondence to:**
A. Mejía,
amejia@engr.psu.edu

**Citation:**
Mejía, A., E. Daly, F. Rossel, T. Jovanovic, and J. Gironás (2014), A stochastic model of streamflow for urbanized basins, *Water Resour. Res.*, *50*, 1984–2001, doi:10.1002/2013WR014834.

Received 1 OCT 2013
Accepted 4 FEB 2014
Accepted article online 8 FEB 2014
Published online 7 MAR 2014

**Abstract** Given the critical role of the streamflow regime for instream, riparian, and floodplain ecosystem sustainability, modeling the long-term effect of urbanization on streamflow is important to predict possible changes in stream ecosystems. Since flow duration curves are largely used to characterize the streamflow regime and define indices for stream ecosystem health, we present two stochastic models, with different levels of complexity, that link the key physical features of urbanized basins with rainfall variability to determine the resulting flow duration curves. The two models are tested against 11 basins with various degrees of urban development, characterized by the percentage of impervious areas in the basin. Results show that the more complex model needs to be used to reproduce accurately the entire flow duration curve. The analysis performed suggests that the transformation of green (i.e., water used in evapotranspiration) to blue (i.e., streamflow) water in urbanized basins is an important long-term source of ecohydrological alteration. The modeling scheme also provides useful links between rainfall variability, urbanization levels, and some streamflow indices of high and low flows.

## 1. Introduction

The health and integrity of instream, riparian, and floodplain ecosystems depend strongly on the full dynamic range of streamflow fluctuations, i.e., the streamflow regime [*Ceola et al*., 2013; *Poff and Zimmerman*, 2010; *Poff et al*., 1997; *Richter et al*., 1996]. Because of this dependency, streamflow has been labeled the "master variable" that limits the distribution and abundance of riverine species [*Power et al*., 1995]. The streamflow regime is a crucial determinant of physical habitat in streams [*Bunn and Arthington*, 2002], it drives ecological processes and successional evolution of riparian plant communities [*Nilsson and Svedmark*, 2002], and it influences nutrient fluxes and cycling [*Pinay et al*., 2002]. Specific findings regarding the strong interdependence between stream ecology and the natural streamflow regime are summarized elsewhere [*Konrad and Booth*, 2005; *Poff and Zimmerman*, 2010; *Poff et al*., 1997]. The streamflow regime is also, directly or indirectly, an essential component of theories in stream ecology (e.g., river continuum [*Vannote et al*., 1980], flood and flow pulse [*Tockner et al*., 2000], and nutrient spiraling [*Doyle*, 2005]) that seek to connect the abiotic and biotic functions of streams.

The implications of anthropogenic perturbations on streamflow regime have been studied in the context of both direct instream perturbations, e.g., dams and diversions [*Botter et al*., 2010; *Poff et al*., 2010; *Richter et al*., 1996], and land-use change, urbanization in particular [*Hamel et al*., 2013; *Poff et al*., 2006]. There is growing evidence that the streamflow regime can be very relevant and useful for understanding the implications of urbanization on stream ecology and ecosystems [*Braud et al*., 2013; *Hamel et al*., 2013; *Hejazi and Moglen*, 2008; *Smakhtin*, 2001]. Although most of the focus of past research has been on the effect that high flows, enhanced by urbanization, have on stream ecology, low flows might also play an important role. Generally, the observation that instream invertebrate diversity and overall invertebrate abundance decrease with increasing urbanization [*Klein*, 1979; *Paul and Meyer*, 2001] is attributed to the increased frequency of higher flows in urbanized basins [*Paul and Meyer*, 2001]. On the other hand, modification of low flows can have important impacts, as discussed by *Groffman et al*. [2003], who suggested that lowering water tables can lead to the presence of a greater proportion of upland tree as opposed to wetland species in the riparian zone. Additionally, in urbanized basins, the streamflow regime can help characterize the interaction between streamflow and water quality [*Nilsson and Renofalt*, 2008; *Shields et al*., 2008], where streamflow

conditions can be associated with stream physicochemical states [*Shields et al*., 2008]. This has important ecological and societal implications in terms of stream health and the availability of freshwater resources [*Falkenmark*, 2003].

To characterize the streamflow regime and its environmental implications, many stream ecohydrological indices have been considered and utilized (e.g., indicators of hydrologic alteration [*Richter et al*., 1996], index of biotic integrity [*Karr*, 1991], ecosurplus and ecodeficit indices [*Gao et al*., 2009], and flashiness index [*Baker et al*., 2004]). However, the interpretation of some of these indices might be difficult, and many of these indices are developed using interrelated quantities, so that their combined use might become redundant [*Gao et al*., 2009; *Olden and Poff*, 2003]. For the sake of simplicity, flow duration curves (FDCs) can be used to represent the streamflow regime and its associated ecological fingerprint [*Smakhtin*, 2001; *Vogel and Fennessey*, 1994]. FDCs have been used extensively in hydrology [*Smakhtin*, 2001], and many of the proposed stream ecohydrological indices can be related to FDCs [*Gao et al*., 2009].

Our aim here is to employ FDCs to describe the streamflow regime of urbanized basins. *Botter et al*. [2007c] presented a stochastic model to derive the statistical properties of streamflow from basins composed by sub-basins with different physical and recession properties. In this study, we apply this model to urbanized basins by differentiating the contribution to the streamflow from pervious and impervious areas. The model permits the derivation of FDCs as a function of parameters associated with rainfall frequency and depth, and coefficients for the recession from the two different areas of the basin. We use the model proposed by *Botter et al*. [2007c] because, for the case of homogeneous natural basins, it has shown good performance and wide applicability for a variety of physical basin-scale conditions. For example, the model has successfully been used to study and characterize the probability distribution of streamflow [*Botter et al*., 2007a, 2007b], flow regimes [*Botter et al*., 2013], flow duration curves and annual minima [*Botter et al*., 2008; *Pumo et al*., 2013], the effect of dams on streamflow variability [*Botter et al*., 2010], the capacity and economic profitability of run-of-river power plants [*Basso and Botter*, 2012; *Lazzaro et al*., 2013], the effect of flow regimes on invertebrate grazing under controlled conditions [*Ceola et al*., 2013], interannual variability in the water balance of a basin [*Zanardo et al*., 2012], annual nutrient load-discharge relationships [*Basu et al*., 2010], and recharge and interflow in the unsaturated zone of a basin [*Thompson et al*., 2011]. Our aim is both theoretically and practically relevant. Theoretically, the model can help synthesize information at the basin scale regarding the interaction between urbanization and hydrologic variability, and thus serves as a unifying framework for understanding change under various macroscopic conditions (climate, geomorphology, terrestrial vegetation, and urbanization). From a practical standpoint, the model permits the quantification of the perturbations induced by the urbanization process on the streamflow regime, and thereby allows a more direct connection between urbanization and environmental degradation.

## 2. Model Description

Our model builds on the framework proposed by *Botter et al*. [2007c] for the stochastic characterization of base flow in heterogeneous natural basins. In what follows, we briefly present the seasonal model of daily rainfall, and its relationship to recharge events from pervious areas and runoff events from impervious areas. We then use this framework in two models, hereinafter referred to as M1 and M2, which differ in the description of the contribution of impervious areas to the streamflow. The models M1 and M2 are described in sections 2.2 and 2.3, respectively.

Two of the main assumptions of M1 and M2 are that (1) rainfall, and thus streamflow, are described at the daily time scale and for a given season (e.g., spring) and (2) urbanized basins can be represented as a combination of pervious and impervious areas, where both areas contribute to the daily generation of streamflow at the outlet of a basin. The pervious areas allow infiltration of rainfall and recharge to the groundwater storage. The amount of recharge is determined by the soil moisture dynamics. In contrast, the presence of impervious areas (e.g., roads, rooftops, parking lots, and sidewalks) can severely restrict soil infiltration and evaporation, and allow for rapid removal of excess rainfall through conventional (connected) storm water infrastructure (SWI) [*Leopold*, 1968; *Walsh et al*., 2012, 2005]. We assume that at the daily time scale the conventional SWI has the main effect of translating the rainfall falling on impervious areas directly to the basin outlet.

By utilizing the daily time scale, the focus here is primarily in changes in the magnitude and timing of streamflow volumes, rather than on the detailed representation of hydrographs or instantaneous peak flows

associated with extreme events. The emphasis on daily streamflow is useful as storm water management is evolving toward the consideration of a wider range of temporal scales [*Petrucci et al*., 2013]. In addition, storage controls for flood events, incorporated as part of the SWI, usually aim for drawdown times no longer than a day; thus their effect can be safely ignored at the daily time scale. Indeed, many studies have found the daily time scale useful in modeling urbanized basins [*Brun and Band*, 2000; *Grimmond et al*., 1986; *Isik et al*., 2013; *Mitchell and Diaper*, 2006; *Mitchell et al*., 2001; *Voinov et al*., 1999].

### 2.1. Urbanized Basins as Stochastic Dynamical Systems

Following *Botter et al*. [2007c], we begin by modeling the series of daily rainfall, $\xi(t)$, as a marked Poisson process, which reads

$$\xi(t)=\sum_{n=1}^{N(t)} y_n \delta(t-t_n), \tag{1}$$

where the sequence $\{t_n\}$ $(n=1,2,\ldots)$ represents the instants of occurrence of $n$ events of the Poisson counting process $N(t)$ $(t \geq 0)$ with mean frequency $\lambda_R$ ($\mathrm{T}^{-1}$), and $\{y_n\}$ is the sequence of independent random rainfall depths $Y$ (L), identically distributed as $h(y)$, and independent of the Poisson process $N(t)$. Rainfall events generate effective rainfall only if the depth of the event, $Y$, is larger than $d_i$ (L), whose value is different for pervious and impervious areas. The pervious threshold $d_P$ (the subscript $P$ denotes pervious conditions), which is related to the soil and vegetation conditions in the basin [*Botter et al*., 2007c], indicates that not all rainfall events contribute to groundwater recharge, while the impervious threshold $d_I$ (the subscript $I$ denotes impervious conditions) can be used to represent the fact that small rainfall events may not contribute to the generation of urban runoff. Accordingly, since we assume the effective daily rainfall to be equal to daily rainfall when it exceeds a constant threshold, the effective rainfall is still a marked Poisson process, with events occurring at a frequency $\lambda_i$ $(\mathrm{T}^{-1})$ that reads [*Laio*, 2006; *Verma et al*., 2011]

$$\lambda_i=\lambda_R\left(1-\int_0^{d_i} h(y)dy\right), \tag{2}$$

and the effective rainfall depths are distributed as

$$h'(y)=\frac{h(y+d_i)}{\int_{d_i}^{+\infty} h(x)dx}. \tag{3}$$

Equations (2) and (3) do not make any assumptions about the probability density function (PDF) for the rainfall depths $Y$ and different PDFs may be considered [see, e.g., *Daly and Porporato*, 2010; *Verma et al*., 2011]. Here we assume that this PDF is exponential [*Botter et al*., 2007c; *Laio et al*., 2001; *Rodriguez-Iturbe et al*., 1999]. Accordingly, the frequency of effective rainfall events in equation (2) is given by $\lambda_i=\lambda_R \exp(-d_i\gamma_R)$, where $\gamma_R^{-1}$ (L) is the mean rainfall depth, and the effective rainfall depths in equation (3) remain exponentially distributed with parameter $\gamma_R$. In the following, the frequency of recharge events from pervious areas is denoted by $\lambda_P$ while the frequency of runoff events from impervious areas is denoted by $\lambda_I$.

Thus, rainfall events with magnitude larger than $d_i$ generate spikes of daily streamflow, which then decreases between runoff events at rates dependent on basin properties. At the outlet of an urbanized basin, the total streamflow, $Q$ ($\mathrm{L}^3/\mathrm{T}$), is then determined by the sum of the contributions due to pervious, $Q_P$ ($\mathrm{L}^3/\mathrm{T}$), and impervious, $Q_I$ ($\mathrm{L}^3/\mathrm{T}$), areas. We will describe the dynamics of these different areas as basins with different thresholds $d_i$ and streamflow recession rates. We will use two different models, M1 and M2, to represent the contribution from impervious areas.

### 2.2. Model M1

We represent the dynamics of the contributions from both pervious and impervious areas within a season using the stochastic differential equation

$$\frac{dQ_i}{dt} = -f_i(Q_i) + \Delta_i \xi_i(t), \tag{4}$$

where $i=P$ for pervious and $i=I$ for impervious contributions. The deterministic term, $f_i(Q_i)$, drives the behavior of the two contributions to streamflow between effective rainfall events; we assume that this term is linear, such that $f_i(Q_i)=k_i Q_i$ $(k_i>0)$. For the pervious contribution, this means that the groundwater storage is modeled as a linear reservoir, where $1/k_P$ (T) takes the meaning of the mean response time. In the case of the impervious contribution, we expect the parameter $k_I$ ($T^{-1}$) to reflect the fast response time typical of conventional storm water drainage. Other studies have successfully made similar storage assumptions for the pervious and impervious contributions [*Coutu et al*., 2012a; *Hejazi and Moglen*, 2008; *McCuen and Snyder*, 1986], but typically within a deterministic context. The constant $\Delta_i$ is equal to $k_P A(1-U)$ and $k_I AU$ for the pervious and impervious contributions, respectively, where $A$ ($L^2$) is the total drainage area of the basin and $U$ is the impervious fraction. $\Delta_i$ ($L^2/T$) accounts for the effect of the recession parameter $k_i$ on the jump size and transforms the rainfall depths into volumes using the contributing drainage area. In essence, equation (4) says that the time evolution of streamflows follows a deterministic trajectory perturbed by jumps of random amplitudes given by $Y_i\Delta_i$. The frequency $\lambda_P$ and $\lambda_I$ of events occurrence of the marked Poisson processes $\xi_P$ and $\xi_I$, respectively, are obtained using the threshold $d_P$ for pervious areas, while $d_I$ is assumed here to be zero, so that every rainfall event contributes to streamflow in proportion to the surface of the impervious areas in the basin.

With the pervious and impervious contributions each defined according to the stochastic dynamics in equation (4), it is possible to obtain the forward master equation for the process, as well as the steady state moment generating function (mgf) for $Q=Q_P+Q_I$ [*Botter et al*., 2007c; *Cox and Miller*, 1965; *Isham et al*., 2005]. The steady state mgf is given by [*Botter et al*., 2007c]

$$p^*(u) = \exp\left\{ -(\lambda_I-\lambda_P)\int_0^\infty \left[1 - \frac{1-\exp\left[-d_P(\gamma_R + k_I AUue^{-k_I t})\right]}{1-\exp\left(-\gamma_R d_P\right)}\left(\frac{\gamma_R}{\gamma_R + k_I AUue^{-k_I t}}\right)\right]dt \right.$$
$$\left. -\lambda_P\int_0^\infty \left[1 - \frac{\gamma_R \exp\left(-k_I AUd_P ue^{-k_I t}\right)}{\gamma_R + u\left(k_I AUe^{-k_I t} + k_P A(1-U)e^{-k_P t}\right)}\right]dt \right\}, \tag{5}$$

where $u$ is a complex variable in the Laplace domain. The derivation of equation (5) is described in *Botter et al*. [2007c]. It does not seem possible to obtain an exact solution for equation (5) and a numerical inversion of the Laplace transform is complicated by the integral terms. The most feasible approach for accessing the PDF in equation (5) is through Monte Carlo simulation. This approach will be used in section 4.

Equation (5) does allow exact solutions for the moments of $Q$. For instance, following the approach in Appendix A, the mean of $Q$ ($\langle Q\rangle_1$ $(L^3/T)$) is given by [*Botter et al*., 2007c]

$$\langle Q\rangle_1 = \frac{\lambda_P}{\gamma_R} A(1-U) + \frac{\lambda_I}{\gamma_R} AU. \tag{6}$$

Based on the marginal distribution for $Q_P$ and $Q_I$, equation (6) states that $\langle Q\rangle_1$ is equal to the sum of the mean pervious, $\langle Q_P\rangle_1 = \lambda_P \gamma_R^{-1} A(1-U)$, and impervious, $\langle Q_I\rangle_1 = \lambda_I \gamma_R^{-1} AU$, contributions. Figure 1a illustrates the behavior of equation (6) as a function of the impervious fraction $U$, which is used to represent changes across an urbanization gradient. Figure 1a shows that $\langle Q_P\rangle_1 \propto (1-U)$ and $\langle Q_I\rangle_1 \propto U$. Thus, $\langle Q_I\rangle_1$ decreases with increasing loss of storage capacity as implied by $1-U$. Relevantly, it has been suggested that the loss of storage capacity is the primary cause behind the various manifestations of hydrological alteration in urbanized basins [*Konrad and Booth*, 2005].

The variance of $Q$ ($\mathrm{var}_1(Q)[(L^3/T)^2]$) is given by [*Botter et al*., 2007c]

$$\mathrm{var}_1(Q) = \frac{\lambda_P k_P (1-U)^2 A^2}{\gamma_R^2} + \frac{\lambda_I k_I A^2 U^2}{\gamma_R^2} + \frac{2\lambda_P k_I k_P A^2 U(1-U)}{\gamma_R^2}\left[\frac{\gamma_R d_P + 2}{k_I + k_P}\right], \tag{7}$$

where the first term represents the pervious contribution, $\mathrm{var}_1(Q_P)$ $((L^3/T)^2)$, the second term the impervious contribution, $\mathrm{var}_1(Q_I)$ $((L^3/T)^2)$, and the third term reflects the interaction between the pervious and

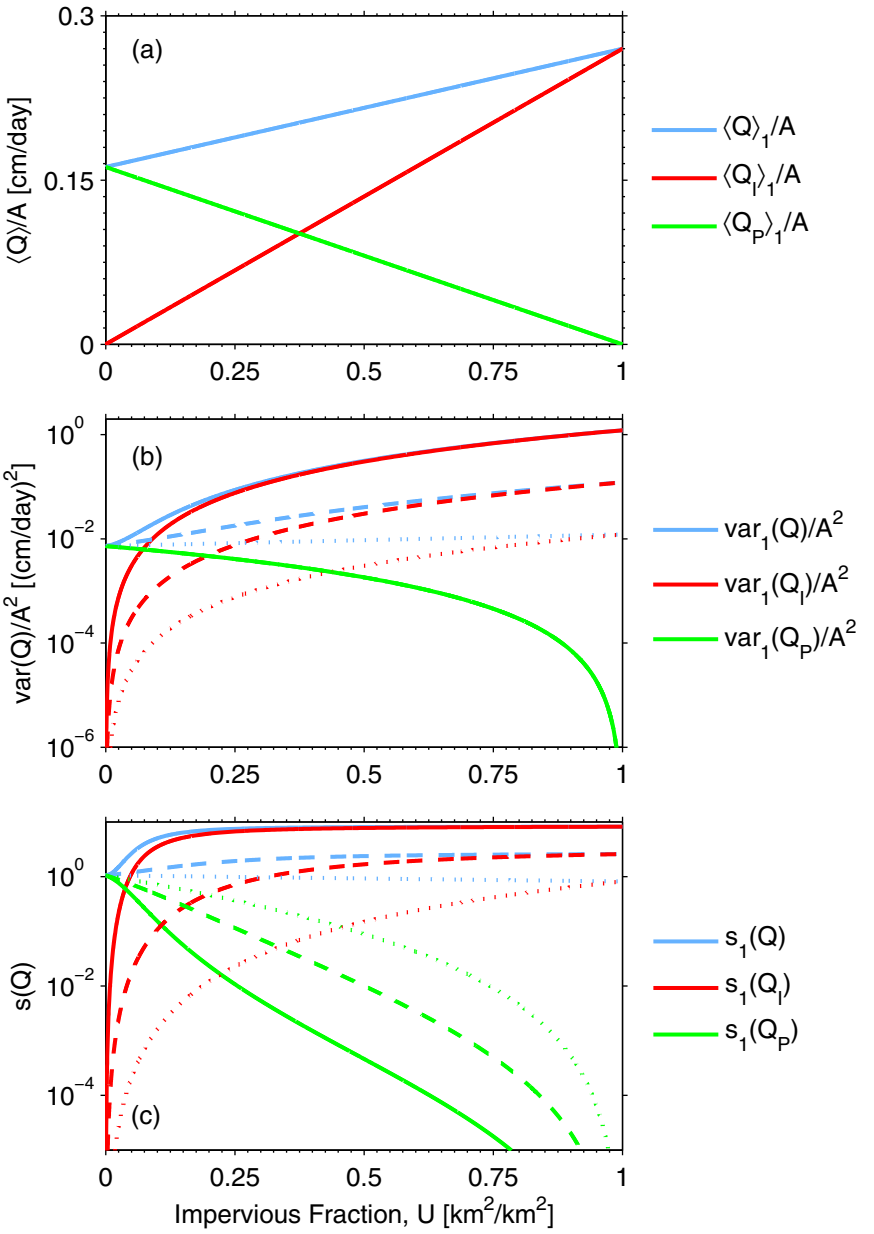


**Figure 1.** (a) Mean, (b) variance, and (c) skewness for M1 as a function of the imperious fraction in the basin. The solid lines correspond to $k_P/k_I=0.01$, the dashed lines to $k_P/k_I=0.1$, and the dotted lines to $k_P/k_I=1$, where $k_P$ is kept constant at 0.05 days$^{-1}$. The mean does not depend on $k_I$ or $k_P$, hence only solid lines are shown in Figure 1a. var $(Q_P)$ in Figure 1b depends only on $k_P$ while $s(Q_P)$ in Figure 1c depends on both $k_I$ and $k_P$. For the remaining parameters, the following values were used: $\lambda_P=0.18$ days$^{-1}$, $\lambda_I=0.3$ days$^{-1}$, and $\alpha_R=0.9$ cm.

impervious contributions. Figure 1b illustrates the behavior of equation (7) using different values of $k_I$. In this figure, when $k_I \gg k_P$, the variance is dominated by var$_1(Q_I)$ and as the difference between $k_I$ and $k_P$ diminishes, the dominance of var$_1(Q_I)$ reduces. Notice that in Figure 1b, the interaction term in equation (7) has an almost negligible effect on var$_1(Q)$. Overall, Figure 1b indicates that for growing levels of urbanization, streamflow variability increases due to the variability induced by impervious areas while the pervious contribution tends to become more uniform or less variable. In Figure 1b, the trend of increasing variability with increasing $U$ corresponds qualitatively with the flashiness condition characteristic of many urbanized basins [see, e.g., *Baker et al.*, 2004].

We also determine the skewness of $Q$, $s_1(Q)$, which is often used as an indicator of hydrologic alteration when characterizing stream ecological conditions [*Olden and Poff*, 2003]; $s_1(Q)$ is given by

$$s_1(Q)=\frac{\langle Q-\langle Q\rangle\rangle_1^3}{\mathrm{var}_1(Q)^{3/2}}, \tag{8}$$

where the third central moment of $Q$, $\langle Q-\langle Q\rangle\rangle_1^3$ $((\mathrm{L/T})^3)$, can be determined from equation (5) (see Appendix A) to yield

$$\begin{aligned}\langle Q-\langle Q\rangle\rangle_1^3=&\frac{2\lambda_P k_P^2 A^3(1-U)^3}{\gamma_R^3}+\frac{2\lambda_I k_I^2 A^3 U^3}{\gamma_R^3}+\\ &\frac{3\lambda_P k_I k_P A^3 U(1-U)}{\gamma_R^3}\left[\frac{2k_P(1-U)(3+d_P\gamma_R)}{(k_I+2k_P)}+\frac{k_I U(6+4d_P\gamma_R+d_P^2\gamma_R^2)}{(2k_I+k_P)}\right].\end{aligned} \tag{9}$$

We use the ratio between the first term in equation (9) and $\mathrm{var}_1(Q)^{3/2}$ as the pervious contribution to the skewness, $s_1(Q_P)$. Likewise, the impervious contribution, $s_1(Q_I)$, is defined as the ratio between the second term in equation (9) and $\mathrm{var}_1(Q)^{3/2}$. The last two terms in equation (9) represent the interaction between the pervious and impervious contributions. This way of separating the skewness does not account for the individual effects of $\mathrm{var}_1(Q_I)$ and $\mathrm{var}_1(Q_P)$ on $s_1(Q)$, but it allows comparison of the relative contribution of the different terms in $\langle Q-\langle Q\rangle\rangle_1^3$ on the basis of $\mathrm{var}_1(Q)^{3/2}$. Figure 1c illustrates $s_1(Q)$ as a function of $U$ using different values of $k_I$. In Figure 1c, the streamflow is positively or right skewed. It becomes increasingly right skewed with increasing urbanization. $s_1(Q)$ is dominated by the contribution from $s_1(Q_P)$ and $s_1(Q_I)$, while the interaction terms have an almost negligible contribution. Further, the marginal distribution of $Q_I$, as well as $Q_P$, is known to be a gamma PDF [*Porporato et al.*, 2004]. Thus, for a fully impervious basin (i.e., $U=1$), $s_1(Q)$ simplifies to the skewness of the gamma distribution, which is $2(\lambda_I/k_I)^{-1/2}$. For high levels of urbanization, the skewness in equation (9) tends to converge to $2(\lambda_I/k_I)^{-1/2}$, converging faster for decreasing values of $k_P/k_I$. This is illustrated in Figure 1c with $k_P/k_I=0.01$; in this case, $s_1(Q)$ and $s_1(Q_I)$ become nearly identical and relatively constant at approximately $U=0.4$. The skewness of the pervious contribution becomes larger with $U$ as $k_P/k_I$ approaches 1.

### 2.3. Model M2

M1 is simplified here to attempt a more amenable mathematical solution. To this end, we describe the seasonal dynamics of $Q$ at the outlet of an urbanized basin with the stochastic differential equation

$$\frac{dQ}{dt}=-kQ+\Delta_P\xi_P(t)+\Delta_I\xi_I(t), \tag{10}$$

where $k$ $(\mathrm{T}^{-1})$ is a recession constant. The constants $\Delta_I$ and $\Delta_P$ are defined as before but now $k=k_I=k_P$, so that $\Delta_I=kAU$ and $\Delta_P=kA(1-U)$. Equation (10) states that the time evolution of streamflows follows a deterministic trajectory $kQ$ perturbed by jumps of random amplitudes given by $Y_I\Delta_I$ and $Y_P\Delta_P$, which are associated with runoff from impervious areas and recharge from pervious areas, respectively. The jumps are simultaneous when $Y > d_P$, otherwise only jumps from impervious areas occur [*Botter et al.*, 2007c]; the threshold $d_I$ is again assumed to be zero.

By separating the dynamics in equation (10) into two independent Poisson processes, the forward master equation for the process can be written as [*Botter et al.*, 2007c; *Cox and Miller*, 1965]

$$\begin{aligned}\frac{\partial p(Q,t)}{\partial t}=&\frac{\partial[kQp(Q,t)]}{\partial Q}-\lambda_I p(Q,t)+(\lambda_I-\lambda_P)\int_0^Q p(Q-z,t)b'(z)dz\\ &+\lambda_P\int_0^Q p(Q-z,t)b''(z)dz,\end{aligned} \tag{11}$$

where $b'(q)$ is the PDF for the jumps when only the impervious areas produce jumps (i.e., $Y < d_P$), and $b''(q)$ is the PDF for jumps when pervious and impervious areas produce jumps simultaneously. To define $b'(q)$, we can use the rainfall PDF and impervious jump $Y_I\Delta_I$ to obtain

$$b'(q)=\frac{\gamma_I}{1-\exp\left[-\gamma_R d_P\right]}\exp\left(\gamma_I q\right)H(kAUd_P-q), \tag{12}$$

where $\gamma_I=\gamma_R/(kAU)$ and $H(\cdot)$ is the Heaviside step function. For $b''(q)$, we use

$$b''(q)=\gamma_P(1-U)\exp\left[-\gamma_P(1-U)(q-kAUd_P)\right]H(q-kAUd_p), \tag{13}$$

where $\gamma_P=\gamma_R/[kA(1-U)]$ (see Appendix B).

Employing the mgf approach as in *Botter et al*. [2007c], the exact solution in the Laplace domain for $p(Q,t\rightarrow\infty)$ in equation (11) is

$$p^*(u)=C(\gamma_I+u)^{-\lambda_I/k}\exp\left\{\frac{\lambda_I}{k}Ei[-d_PAUk(\gamma_I+u)]-\frac{\lambda_P}{k}\exp\left(\gamma_R d_P U\right)Ei[-d_PAUk(\gamma_I U+u)]\right\}, \tag{14}$$

where $Ei(\cdot)$ is the exponential integral function [*Abramowitz and Stegun*, 1964] and the normalization constant $C$ is given by

$$C=\left(\frac{AUk}{\gamma_R}\right)^{-\lambda_I/k}\exp\left[\frac{\lambda_I}{k}Ei(-d_P\gamma_R)-\frac{\lambda_P}{k}\exp\left(\gamma_R d_P U\right)Ei(-d_P\gamma_R U)\right]. \tag{15}$$

Since it does not seem possible to invert equation (14) analytically, we will use numerical methods for the inversion [*Valkó and Abate*, 2004].

Equation (14) allows analytical solutions for the moments of $Q$. Using equation (14) and the cumulant generating function (Appendix A), the steady state mean, variance, and third central moment of $Q$ can be calculated as

$$\langle Q\rangle_2=\langle Q\rangle_1, \tag{16}$$

$$\mathrm{var}_2(Q)=\frac{kA^2}{\gamma_R^2}\left[\lambda_P(1-U^2)+\lambda_I U^2+\lambda_P(1-U)Ud_P\gamma_R\right],\ \text{and} \tag{17}$$

$$\langle Q-\langle Q\rangle\rangle_2^3=\frac{2A^3k^2\lambda_P(1-U^3)}{\gamma_R^3}+\frac{2A^3k^2\lambda_I U^3}{\gamma_R^3}+\frac{2A^3d_Pk^2\lambda_P U}{\gamma_R}\left[\frac{(1-U^2)}{\gamma_R}+\frac{d_PU(1-U)}{2}\right]. \tag{18}$$

The skewness $s_2(Q)$ is given by $\langle Q-\langle Q\rangle\rangle_2^3/\mathrm{var}_2(Q)^{3/2}$. Figures 2a and 2b illustrate the behavior of $\mathrm{var}_2(Q)$ and $s_2(Q)$, respectively, using different values of $k$. In this figure, we only consider the effect of the parameter $k$ on the variance and skewness because previous results indicate that $k$ has a more dominant role than other parameters, such as $\lambda_P$ and $\lambda_I$ [*Botter et al*., 2007c]. Figure 2 helps to highlight some main differences, as well as similarities, between M1 and M2. Figure 2 shows that for $U=0$ and $U=1$ with $k=k_P$ and $k=k_I$, respectively, the two models result in the same value for the variance and skewness, while these values tend to differ in the range $0<U<1$. For example, for $k=(k_P+k_I)/2$ in Figure 2a, the variance of the two models is only the same at approximately $U=0.6$. One main difference between M1 and M2 in Figure 2 is that having a single recession parameter for M2 tends to smooth out the range of variability of the variance and skewness. In other words, having a slow and fast response time for the pervious and impervious areas, respectively, results in a larger range of variability for the variance and skewness of M1 across values of $U$.

## 3. Case Studies

To study the ability of M1 and M2 to represent streamflow dynamics in urbanized basins, we use data from 11 basins situated in the metropolitan areas of the cities of Baltimore and Washington, D. C. The location of the basins and their main urban land-use categories is illustrated in Figure 3. Table 1 summarizes the main characteristics of the selected basins. The Baltimore-Washington, D. C region as a whole has experienced steady urban growth in the last decades. An advantage of working with this region is that data is available

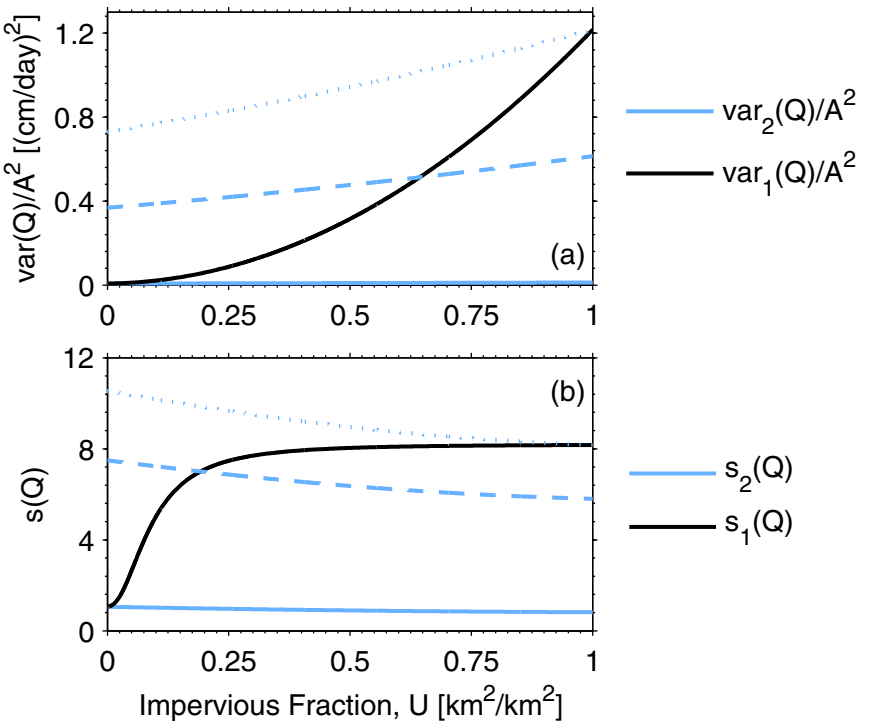


**Figure 2.** Comparison between the (a) variance and (b) skewness of M1 and M2 as a function of the impervious fraction in the basin. The solid lines are for $k=k_P$, the dashed lines for $k=(k_P+k_I)/2$, and the dotted lines for $k=k_I$, where $k_P=0.05$ days$^{-1}$ and $k_I=5$days$^{-1}$. The remaining parameter values are the same as in Figure 1.

to describe the annual time evolution of the urbanization process. This allows us to match specific time periods in the streamflow record to a given level of urbanization, and to identify time periods where urban growth is relatively mild. The land-use data set is described in *Beighley and Moglen* [2003].

The Baltimore-Washington, D. C. region is characterized by a humid temperate climate. The mean annual precipitation and runoff are roughly 109 and 41 cm, respectively, with the difference between the two being attributed mainly to evapotranspiration losses [*Moody*, 1986; *Rutledge and Mesko*, 1996]. The general seasonal pattern is for monthly mean streamflows to decrease from highs in March to lows in August or September [*Doheny*, 1999; *Froelich et al*., 1980; *Moody*, 1986]. The latter is typically accompanied by increasing evapotranspiration losses and decreasing groundwater discharge to streams [*Doheny*, 1999]. In terms of physiographic conditions, all the basins lie in the Piedmont physiographic province, have mild sloped terrain, and are underlain primarily by crystalline bedrock [*Fenneman*, 1938; *Rutledge and Mesko*, 1996]. A small downstream portion of Stemmers Run and Whitemarsh Run is in the Atlantic Coastal Plain physiographic province, which is underlain by unconsolidated layers of sand, gravel, silt, and clay [*Rutledge and Mesko*, 1996].

The selected basins have drainage areas that range from 5.5 to 98.4 km$^2$, and the fraction of basin impervious area ranges from 5.2 to 36.05% of the total drainage area (Table 1). The pervious land in the basins is predominantly agricultural and urban grassed areas, with riparian corridors being typically forested. The impervious areas are predominantly residential and roads with some commercial areas. Although rainfall tends to be distributed relatively uniformly throughout the year, we employ M1 and M2 at the seasonal level because streamflow, and base flow in particular, tends to exhibit a seasonal dependency [*Moody*, 1986; *Rutledge and Mesko*, 1996]. To illustrate the application of M1 and M2, we chose the spring (wet) season (from the beginning of February to the end of April), where the influence of urbanization may be more accentuated than in the other seasons.

The streamflow data were obtained from the U.S. Geological Survey and the rainfall data from NOAAs National Climatic Data Center. The location of the streamflow and rainfall gages is illustrated in Figure 3 and the gage numbers are summarized in Table 1. For the wet season, the basins have a mean daily rainfall of

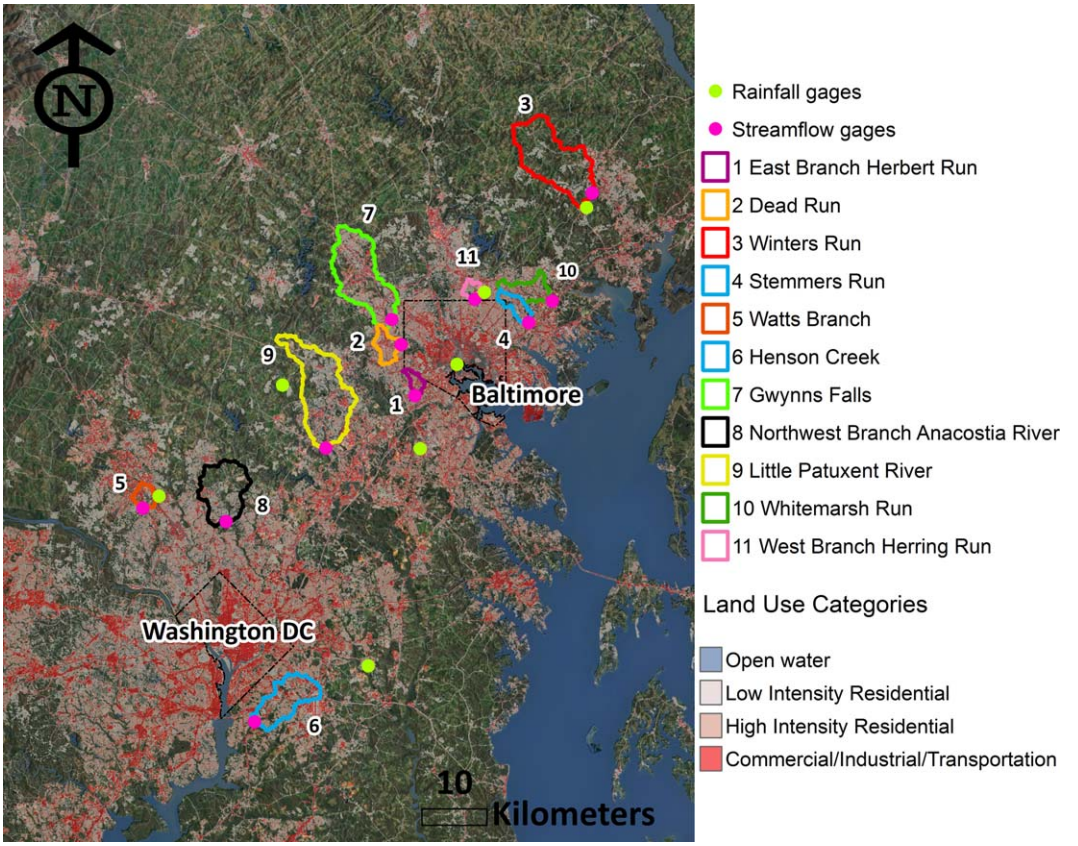


**Figure 3.** Map of the Baltimore-Washington, D. C. region illustrating the location of the basins used in this study and their associated rainfall and streamflow gages. The background image shows the regional distribution of urban land use (c. 2001) over an areal photograph of the region.

0.885 cm and a mean rainfall frequency of 0.338 days$^{-1}$ (Table 1). The period of analysis for each basin is included in Table 1. These periods were selected to maintain urban growth within each basin relatively low, avoid long stretches of missing data, retain at least 10 years of streamflow data, and reflect storm water conditions prior to the year 2000, which marks the transition to more comprehensive storm water management practices within the study area, i.e., from connected to more disconnected SWI.

## 4. Results and Discussion

This section is divided into four parts. First, we compare M1 against the observed streamflow and assess its performance. Second, we compare M2 against both the observed streamflow and M1. Third, we examine the behavior of the moments of the streamflow $Q$ across an urbanization gradient. Fourth, we illustrate the

**Table 1.** Summary of Data and Parameter Values

| Streamflow Gage | Rainfall Gage | Basin Name | Period of Analysis | $A$ (km$^2$) | $\langle Q \rangle / A$(cm /day ) | $\gamma_R^{-1}$(cm ) | $\lambda_R$ (1/day) | $U$ (%) |
|---|---|---|---|---|---|---|---|---|
| 01589100 | 18–0465 | East Branch Herbert Run | 1974–1984 | 6.4 | 0.159 | 0.829 | 0.340 | 35.75 |
| 01589330 | 18–0470 | Dead Run | 1964–1974 | 14.3 | 0.159 | 0.909 | 0.316 | 30.00 |
| 01581700 | 18–0732 | Winters Run | 1980–1995 | 90.1 | 0.181 | 0.88 | 0.352 | 5.20 |
| 01585300 | 18–8877 | Stemmers Run | 1977–1989 | 11.6 | 0.190 | 0.898 | 0.362 | 30.00 |
| 01645200 | 18–7705 | Watts Branch | 1968–1979 | 9.6 | 0.145 | 0.841 | 0.317 | 25.05 |
| 01653500 | 18–9070 | Henson Creek | 1955–1966 | 43.3 | 0.170 | 0.917 | 0.305 | 28.00 |
| 01589300 | 18–0470 | Gwynns Falls | 1973–1986 | 84.2 | 0.166 | 0.909 | 0.316 | 20.35 |
| 01650500 | 18–7705 | Northwest Branch Anacostia River | 1972–1982 | 54.6 | 0.155 | 0.841 | 0.317 | 8.75 |
| 01593500 | 18–1862 | Little Patuxent River | 1987–1997 | 98.4 | 0.163 | 0.843 | 0.347 | 21.40 |
| 01585100 | 18–8877 | Whitemarsh Run | 1988–2000 | 19.7 | 0.212 | 0.898 | 0.362 | 34.10 |
| 01585200 | 18–0470 | West Branch Herring Run | 1970–1986 | 5.5 | 0.150 | 0.909 | 0.316 | 36.05 |

**Table 2.** Summary of Additional Parameter Values, Objective Function, and Index of Model Performance for M1 and M2

| Streamflow Gage | $\lambda_P$ (1/day) | $k_I$ (1/day) | $k_P$ (1/day) | OF (M1) (log(cm/day)) | $r$ (M1) | $k$ (1/day) | OF (M2) (log(cm/day)) | $r$ (M2) |
|---|---|---|---|---|---|---|---|---|
| 01589100 | 0.106 | 3.041 | 0.012 | 5.65 | 0.96 | 0.161 | 37.65 | 0.79 |
| 01589330 | 0.109 | 8.628 | 0.060 | 18.02 | 0.89 | 0.238 | 45.05 | 0.81 |
| 01581700 | 0.216 | 9.982 | 0.045 | 11.54 | 0.98 | 0.057 | 15.45 | 0.89 |
| 01585300 | 0.167 | 9.920 | 0.085 | 22.90 | 0.93 | 0.319 | 47.75 | 0.80 |
| 01645200 | 0.132 | 5.110 | 0.019 | 5.46 | 0.98 | 0.109 | 30.99 | 0.74 |
| 01653500 | 0.129 | 1.657 | 0.019 | 2.10 | 0.97 | 0.085 | 19.05 | 0.89 |
| 01589300 | 0.140 | 5.613 | 0.026 | 7.65 | 0.98 | 0.085 | 26.14 | 0.76 |
| 01650500 | 0.173 | 9.931 | 0.055 | 17.53 | 0.97 | 0.077 | 25.00 | 0.78 |
| 01593500 | 0.170 | 5.396 | 0.022 | 4.18 | 0.99 | 0.099 | 25.72 | 0.68 |
| 01585100 | 0.154 | 5.972 | 0.056 | 15.20 | 0.91 | 0.236 | 39.91 | 0.81 |
| 01585200 | 0.099 | 1.366 | 0.012 | 7.52 | 0.98 | 0.170 | 26.42 | 0.87 |

determination of stream ecohydrological indices with M1. Before applying the models, we satisfactorily verified that the distribution of daily rainfall depths in the wet season was reasonably close to exponential.

### 4.1. Comparison Between M1 and the Observed Streamflow

Since we are interested in the statistical properties of streamflow, we use FDCs to compare M1 against the observed streamflow [*Smakhtin*, 2001; *Vogel and Fennessey*, 1994]. We thus generated streamflow series via Monte Carlo simulations with M1 and then estimated the empirical FDCs. The application of M1 requires the value of eight parameters ($A$, $U$, $\gamma_R$, $\lambda_R$, $\lambda_I$, $\lambda_P$, $k_I$, and $k_P$), most of which can be determined directly from the available data sets. The parameters $\gamma_R$ and $\lambda_R$ (Table 1) were obtained from the daily rainfall data in the wet season; $\lambda_I$ was set equal to $\lambda_R$, and $\lambda_P$ was estimated using equation (6) and the mean observed streamflow. The values of $\lambda_P$ used are reported in Table 2. Alternatively, $\lambda_P$ and $\lambda_I$ can be estimated from equation (2) if the thresholds $d_P$ and $d_I$, respectively, are known. The thresholds $d_P$ and $d_I$ can be estimated from rainfall statistics and physical features of the basin, as proposed by *Botter et al*. [2007a]. The recession parameters, $k_I$ and $k_P$, are difficult to estimate from the available data. The very few studies that have investigated the effect of anthropogenic perturbations on streamflow recessions indicate that common approaches to recession analysis can misrepresent recessions in human dominated basins [*Wang and Cai*, 2010]. Thus, we tuned up the values of both $k_I$ and $k_P$ to improve the fit between the modeled and observed FDCs using nonlinear optimization [*Byrd et al*., 1999]. For the optimizations, we used the sum of the absolute distance, in log scale, between the modeled and observed FDC as the objective function (OF). The optimized values for $k_I$ and $k_P$ are reported in Table 2. The values of $k_I$ vary from 1.366 to 9.982 days$^{-1}$ while $k_P$ varies from 0.012 to 0.085 days$^{-1}$. The values obtained for both $k_I$ and $k_P$ are within the range of variability of previously reported values [*Botter et al*., 2013, 2010; *Coutu et al*., 2012b]. The variability of $k_P$ has been discussed elsewhere [see, e.g., *Botter et al*., 2007c, 2013]. The variability of $k_I$ can be partially dependent on the way imperviousness is distributed within a basin. For example, *Beighley and Moglen* [2003] found that when imperviousness is located mostly upstream, rather than near the main basin outlet, streamflow peaks tend generally to be larger and response time longer at the main outlet. This and other factors, such as the characteristics of the SWI [*Gironas et al*., 2009], are likely to influence the variability of $k_I$.

Following the parameter estimation approach just described, we determined the FDCs for all the basins in this study. Figures 4a–4c compare the modeled and observed FDC for three of the selected basins. From visual inspection, Figures 4a–4c show good agreement between M1 and the observed streamflow. We also used the following index of performance to quantify the performance of the FDCs [*Claps et al*., 2005]:

$$r = 1 - \frac{D^2}{\mathrm{var}\,(Q)}, \tag{19}$$

where $D^2$ ($(L^3/T)^2$) is the mean squared distance between the observed and modeled FDC and $\mathrm{var}\,(Q)$ ($(L^3/T)^2$) is the variance of the observed streamflow. A value of $r=1$ indicates a perfect fit. Table 2 summarizes the values of $r$ and OF. We employ the index in equation (19) because it can be interpreted more easily than OF. The values of $r$ in Table 2 indicate a good performance for all the modeled FDCs. The average $r$ value is 0.96 and the range is from 0.89 to 0.99. Further, we show in Figures 4d–4f quantile-to-quantile plots

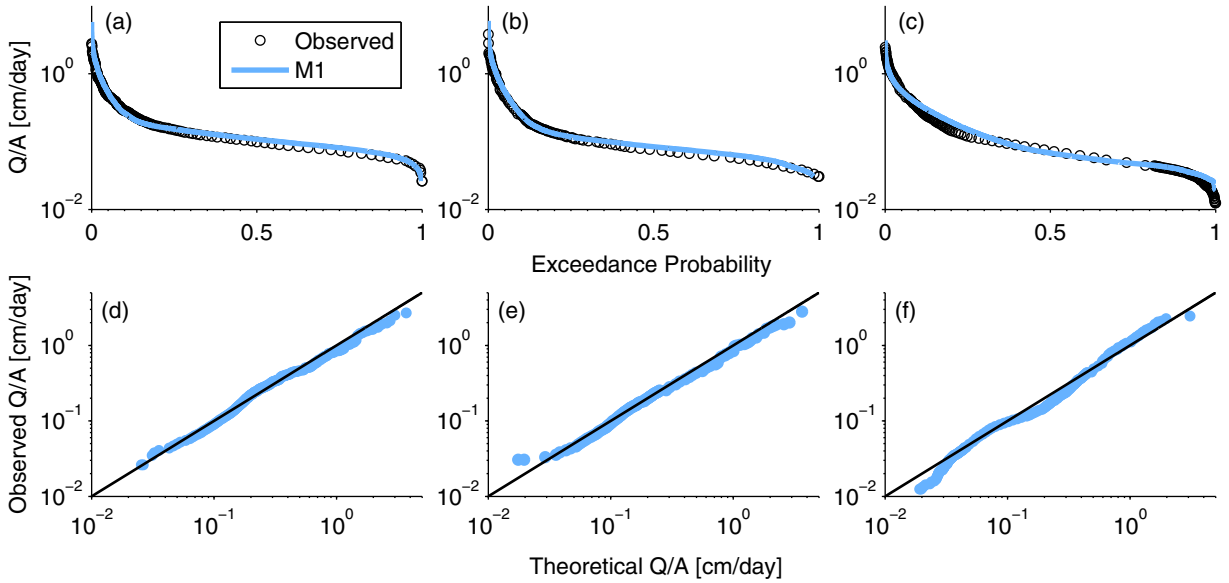


**Figure 4.** Comparison between the FDC for M1 and the observed streamflow at (a) Gwynns Falls (USGS streamflow gage 01589300), (b) Watts Branch (USGS streamflow gage 01645200), and (c) West Branch Herring Run (USGS streamflow gage 01585200). Quantile-to-quantile plots for M1 at (d) Gwynns Falls, (e) Watts Branch, and (f) West Branch Herring Run. The comparisons are for the wet season (from February to April).

(q-q plots) for the same three basins in Figures 4a–4c. The q-q plots confirm that the fits between modeled and observed FDCs are reasonable.

Thus, M1 is able to reproduce the FDCs for streamflow during the wet season in the urbanized basins of this study. The parameters in M1 can be determined from readily available data sets, with the exception of the two recession parameters that need to be calibrated. The main feature of M1 is its ability to describe the streamflow regime of an urbanized basin while embedding key information about rainfall variability, and the main physical drivers and underlying basin-scale conditions.

### 4.2. Comparison Between M1 and M2

We explore here the ability of M2 to describe streamflow fluctuations in urbanized basins by comparing it against the observed streamflow and M1. We will illustrate the behavior of M2 using two different cases from Table 1, one for a heavily urbanized basin (East Branch Herbert Run) and another one for a basin with little urbanization (Winters Run).

To compare M2 against the observed streamflow, we need first to determine the recession parameter, $k$. The remaining parameters required by M2 can be determined from the values reported in Tables 1 and 2. To estimate $k$, we used two different methods. The first method applies the same optimization procedure used previously for M1. The second method uses the optimized values of $k_I$ and $k_P$ to estimate $k$ and it is used to better understand the behavior of $k$ in M2. Figure 5 compares the results from both methods against M1 and the observed FDC. In Figure 5a, when using the first method, M2 is not able to match the observed high and intermediate streamflow values, while matching the low streamflow values. In contrast, M1 is able to fully reproduce the observed FDC. Using the second method, where $k$ was set equal to $k_I$, M2 is now only able to match the observed high streamflow values. We used $k_I$ to estimate $k$ in Figure 5a because this is a heavily urbanized basin and we can expect $k_I$ in this case to have a strong influence on the streamflow. Notice that the value of $k$ in the second method ($k=3.041$ days$^{-1}$ from Table 2) is much larger than the value in the first method ($k=0.161$ days$^{-1}$ from Table 2). Thus, to fully represent the observed FDC, it is necessary to capture two different characteristic time scales, one associated with the fast response of impervious areas and another one with the slow response of pervious areas. For comparison purposes, the calibrated values of $k$ for all the basins in this study, as well as the associated values of OF and $r$, are reported in Table 2.

Figure 5b illustrates another comparison between M2 and the observed streamflow. For this comparison, we used $k=k_P$ for the second method because the basin in Figure 5b has a relatively low level of

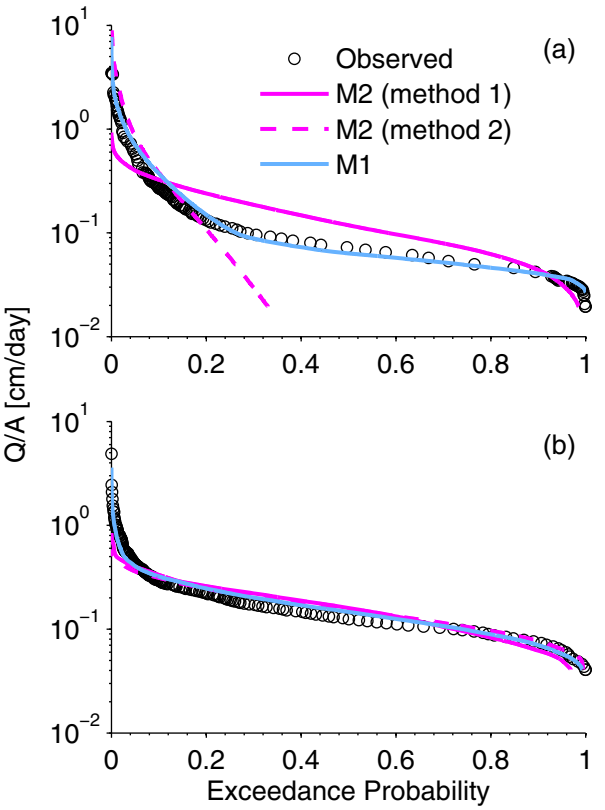


**Figure 5.** FDC for M1, M2, and the observed streamflow at (a) East Branch Herbert Run (USGS streamflow gage 01589100) and (b) Winters Run (USGS streamflow gage 01581700). M2 (method 1) uses the optimized value of $k$ while M2 (method 2) uses $k$ equal to $k_I$ and $k_P$ for Figures 5a and 5b, respectively. In Figure 5b, the FDC for M2 (method 1) and M2 (method 2) is nearly the same. The comparison is for the wet season.

urbanization (5.2% imperviousness). In this case, M2 is able to match the observed FDC for all the exceedance probabilities >0.1. M1 is again able to capture the entire range of streamflows (Figure 5b). The difference between M2 estimated using the first and second methods is now practically negligible. Figures 5a and 5b suggest that the distinction between pervious and impervious contributions to the streamflow can be hydrologically important when dealing with relatively high levels of urbanization.

In summary, M2 behaves similar to M1 when there is little urbanization involved. As the level of urbanization increases, M2 tends to deviate from M1. Ultimately, the relative contribution from impervious and pervious areas as well as the difference in their response times (e.g., $1/k_I$ and $1/k_P$) determine the streamflow regime of the urbanized basins investigated here.

### 4.3. Moments of the Streamflow Q Along an Urbanization Gradient

We analyze with M1 the behavior of the streamflow moments (i.e., mean, variance, and skewness) along an urbanization gradient. The gradient is defined based on the basins used in this study. Figure 6a illustrates the mean streamflow as a function of $U$. In Figure 6a, $\langle Q_P \rangle_1$ tends to decrease and $\langle Q_I \rangle_1$ to increase with increasing $U$, while $\langle Q \rangle_1$ exhibits greater variability and no apparent trend with increasing $U$. These trends are further illustrated in Figure 6a (solid lines) using equation (6). The parameters for equation (6) were determined from the arithmetic average of the parameter values for all the basins in this study. The behavior of $\langle Q_P \rangle_1$ and $\langle Q_I \rangle_1$ in Figure 6a suggests that pervious areas can play a significant role in the long-term behavior of urbanized basins, given that their contribution to $\langle Q \rangle_1$ is larger than $\langle Q_I \rangle_1$ for most of the values of $U$ examined here. To illustrate this point further, we use the dimensionless ratio between the mean streamflow and the mean rainfall on the basin which is given by

$$\langle \bar{Q} \rangle_1 = \frac{\gamma_R}{\lambda_R A} \langle Q \rangle_1 . \tag{20}$$

Using equations (6) and (20) and recalling that we assumed $\lambda_I = \lambda_R$, the sensitivity of $\langle \bar{Q} \rangle_1$ to an instantaneous change in impervious cover is

$$\frac{d\langle \bar{Q} \rangle_1}{dU} = 1 - \phi, \tag{21}$$

where $\phi = \lambda_P / \lambda_R$ approximately represents the fraction of water not used by vegetation (i.e., blue water) and $1-\phi$ is the fraction used by vegetation (i.e., green water). Hence, the effect of the perturbations induced by $U$ on the streamflow depends on the green water and thereby on the terrestrial vegetation cover in the basin. Interestingly, this also suggests that the perturbations are dependent on the definition of an appropriate baseline condition prior to urbanization.

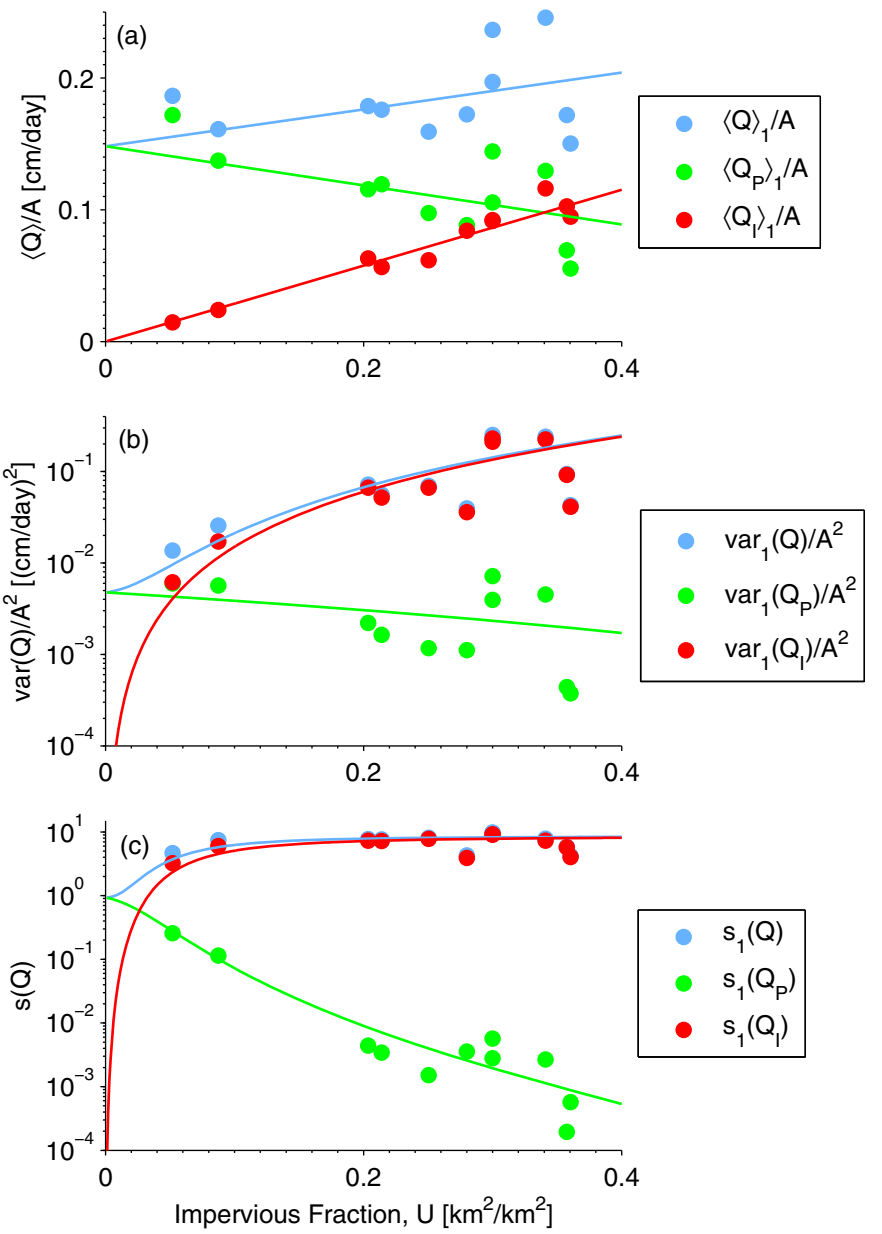


**Figure 6.** (a) Mean, (b) variance, and (c) skewness for the urbanized basins in this study using M1 (wet season). The moments are shown as a function of the impervious fraction in the basin to illustrate changes across an urbanization gradient. The solid lines are the analytical moments for M1 (blue), and their associated pervious (green) and impervious (red) contributions, using average parameter values. The average parameters were determined from the parameter values for the 11 basins used in this study. Each dot in the figure corresponds to one of the 11 urbanized basins used in this study.

The results for $\mathrm{var}_1(Q)$ are illustrated in Figure 6b. Figure 6b, which shows a pattern similar to the one implied by equation (7) (solid lines in Figure 6b), indicates that $\mathrm{var}_1(Q_I)$ increases rapidly with $U$ and tends to dominate the value of $\mathrm{var}_1(Q)$, while $\mathrm{var}_1(Q_P)$ decreases with $U$ and contributes little to $\mathrm{var}_1(Q)$. These results support the utility of $\mathrm{var}_1(Q)$ as an indicator of the influence of $U$ on streamflows. Additionally, $\mathrm{var}_1(Q)$ helps identify other factors that control the flashiness of urban streams. For example, the term $\mathrm{var}_1(Q_I)$ in equation (7) indicates that streamflows become more flashy when $k_I$ increases (i.e., the response time of urban areas decreases) and/or the mean rainfall increases.

In Figure 6c, the results for $s_1(Q)$ are also similar to the theoretical results implied by equations (8) and (9). Figure 6c indicates that $s_1(Q)$ is controlled by $s_1(Q_I)$ across values of $U$ and that $s_1(Q)$ reaches an approximately constant value after a relatively low level of urbanization. In this regard, $s_1(Q)$ is less effective than

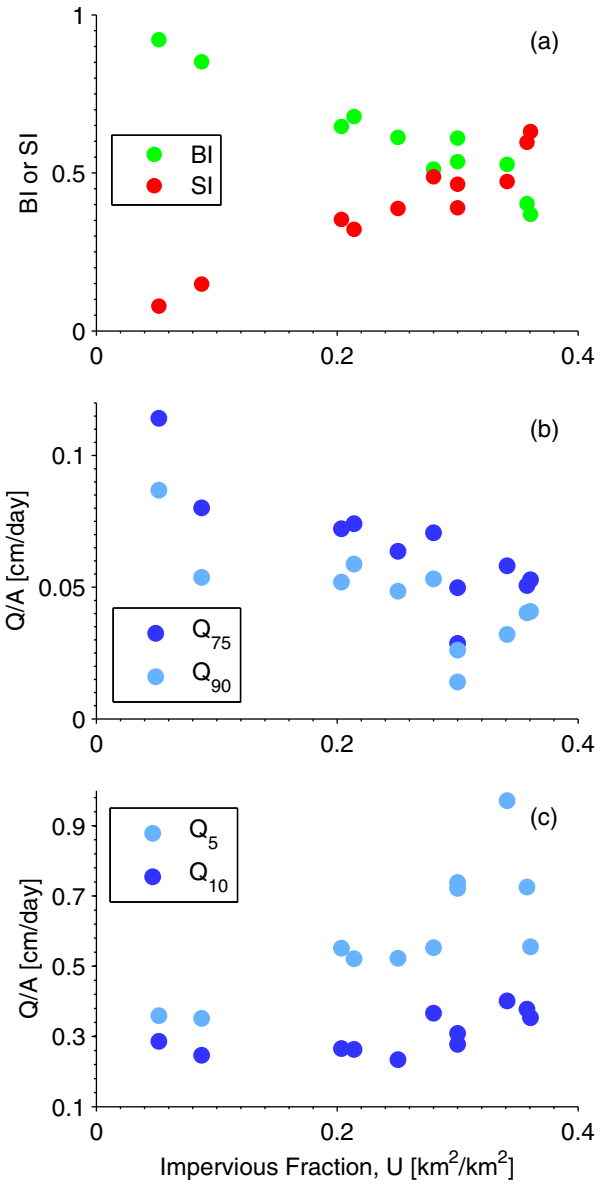


**Figure 7.** Ecohydrological indices using M1 (wet season): (a) stormflow (*SI*) and base flow (*BI*) indexes, (b) low flows ($Q_{75}$ and $Q_{90}$ are the streamflow values with 0.75 and 0.90 exceedance probability, respectively), and (c) high flows ($Q_5$ and $Q_{10}$ are the streamflow values with 0.05 and 0.1 exceedance probability, respectively). Each dot in the figure corresponds to one of the 11 urbanized basins used in this study.

$\mathrm{var}_1(Q)$ in quantifying broad changes along an urbanization gradient. Thus, if $s_1(Q)$ is used to quantify impacts to stream ecology, it will likely be most useful for sensitive taxa that can be affected by low levels of urbanization.

### 4.4. Stream Ecohydrological Indices Along an Urbanization Gradient

A large number of ecohydrological indices have been proposed to synthesize the streamflow regime in ways that are meaningful to stream ecosystems [*Clausen and Biggs*, 1997; *Poff and Allan*, 1995; *Poff et al.*, 1997; *Richter et al.*, 1996]. From extensive analysis of stream ecohydrological data, *Konrad and Booth* [2005] suggested that most of these indices can be classified into four main types of hydrologic alterations: (1) increased daily variation in streamflow, (2) redistribution of water from base flow to stormflow, (3) reductions in low flows, and (4) increased frequency of high flows. We already represented the type 1 alterations in section 4.3 using $\mathrm{var}_1(Q)$. The remaining types are illustrated here using the model M1.

To represent the type 2 alterations, we use the base flow index (*BI*) [*Klein*, 1979] which is here defined as $\langle Q_P \rangle_1 / \langle Q \rangle_1$ such that

$$BI = \frac{\phi(1-U)}{[\phi + U(1-\phi)]}, \tag{22}$$

Equation (22) says that *BI* is the ratio between the mean streamflow contribution from pervious areas and the total mean streamflow. The total mean streamflow can be seen as the sum of the blue water in the basin ($\phi$), from both pervious and impervious areas, plus the green water that is converted into runoff due to the presence of impervious areas ($U(1-\phi)$). Figure 7a illustrates *BI* along the urbanization gradient from the basins in this study. In this figure, *BI* decreases with increasing *U*, highlighting the key role that the loss of storage capacity ($1 - U$) can play in urbanized basins. The results presented here for *BI* are consistent with previous studies for the same region [*Brun and Band*, 2000; *Klein*, 1979; *Moglen et al.*, 2004].

Alternatively, we can define a stormflow index *SI* as $SI = 1 - BI$. Using equation (22) and recalling that $\lambda_I = \lambda_R$, *SI* can be expressed as

$$SI = \frac{U}{[\phi + U(1-\phi)]}. \tag{23}$$

*SI* measures the fraction of urban runoff relative to the total mean streamflow, and its relationship with *U* is illustrated in Figure 7a. *BI* and *SI* highlight the potential of urbanized basins to redistribute water.

To illustrate the type 3 and 4 alterations, we use FDCs and common indices of streamflow alteration, such as the streamflow values that are exceeded 5% ($Q_5$), 10% ($Q_{10}$), 75% ($Q_{75}$), and 90% ($Q_{90}$) of the time. These indices can be calculated from the observed streamflow time series; however, given the good agreement between the observed FDCs and the ones calculated with the model M1, we show in Figures 7b and 7c the results from the model. In Figure 7b, the indices $Q_{75}$ and $Q_{90}$ are shown as a function of $U$. These indices are commonly used to quantify low flow alterations [*Clausen and Biggs*, 1997; *Poff and Allan*, 1995]. In Figure 7b, both $Q_{75}$ and $Q_{90}$ tend to decrease with increasing $U$. Similar results, in terms of historical minimum flows, were reported by *Hejazi and Moglen* [2007] for urbanized basins in the same region. For the type 4 alterations, we exhibit in Figure 7c the $Q_5$ and $Q_{10}$ indices as function of $U$. These are both common indices of frequent high flows. In Figure 7c, $Q_5$ and $Q_{10}$ tend to increase with $U$ but the trend is more apparent for $Q_5$. The behavior of the low ($Q_{75}$ and $Q_{90}$) and high flow ($Q_5$ and $Q_{10}$) indices in Figure 7 has relevant ecological implications [*Clausen and Biggs*, 1997; *Poff and Allan*, 1995]. For example, decreasing trends in $Q_{90}$ tend to be associated with less periphyton and invertebrate density, while increasing trends in $Q_5$ and $Q_{10}$ tend to be associated with dominance of trophic and habitat generalists in fish assemblages [*Clausen and Biggs*, 1997; *Poff and Allan*, 1995]. Indeed, stream studies in the Maryland Piedmont suggest that increasing urbanization has resulted in lower abundance and diversity of macroinvertebrate and fish species [*Klein*, 1979; *Moore and Palmer*, 2005; *Morgan and Cushman*, 2005].

## 5. Conclusions

We used a stochastic model to describe and analyze the streamflow regime of urbanized basins. We applied the model to urbanized basins in the Baltimore-Washington, D. C region, where historical land use data are available and urban growth has contributed considerably in the last decades to increase the regional extent of urban land cover. We examined basins with varying levels of impervious cover. On the basis of the analysis performed, the following conclusions are emphasized:

1. The proposed modeling approach is able to capture some of the most common hydrological perturbations associated with increasing urbanization. For instance, it shows an increase in variance (flashiness) with increasing urbanization. It also shows that rainfall and stormflow, as well as the partitioning of streamflow into stormflow and base flow, are highly interdependent phenomena in urbanized basins. Ultimately, the modeling approach indicates that the urbanization process can have an influential effect on FDCs.

2. We found a consistent link between the statistical properties characterizing the streamflow regime (i.e., mean, variance, and skewness) and the degree of urban development. This may be useful when assessing the dynamic impacts of urbanization as it takes place in time.

3. The model also permits to link rainfall variability, both in terms of frequency and magnitude, and the degree of urbanization to obtain indices of high and low flows, which are often used as ecohydrological indices of stream health.

4. The transformation of green to blue water induced by the urbanization process is an important characteristic of the long-term hydrological behavior of urbanized basins. This is seldom recognized but may be a helpful source of progress in storm water management policy. For instance, this transformed water, or at least some of it, could be managed separately and used for different purposes, including meeting human needs, with potentially reduced impacts to downstream ecosystems dependent on basin streamflow.

## Appendix A: Moments of the Streamflow $Q$

By taking the natural logarithm of equation (5), we obtain the cumulant generating function (cgf) of $p^*(u)$. With the cgf, the mean, variance, and third central moment of $Q$ can be determined as

$$\langle Q \rangle = -\left.\frac{\partial R(u)}{\partial u}\right|_{u=0}, \tag{A1}$$

$$\mathrm{var}\,(Q) = \left.\frac{\partial^2 R(u)}{\partial u^2}\right|_{u=0}, \text{ and} \tag{A2}$$

$$\langle Q-\langle Q\rangle\rangle^3=-\left.\frac{\partial^3 R(u)}{\partial u^3}\right|_{u=0}, \tag{A3}$$

where $R(u)=\ln[p^*(u)]$.

## Appendix B: Probability Density Function for the Streamflow Jumps

To obtain the PDF for the total streamflow jump $q$ when $Y > d_P$, we start with the PDF for the jumps from pervious areas ($q_P$):

$$b''(q_P)=\gamma_P \exp(-\gamma_P q_P)H(q_P), \tag{B1}$$

where $\gamma_P=\gamma_R/[kA(1-U)]$). Additionally, when $Y > d_P$, the total streamflow jump can be expressed as

$$q=q_P+q_I, \tag{B2}$$

where $q_I$ is the jump from impervious areas. To express (B2) as a function of $q_P$ alone, we use $q_I=Y_I kAU$ and $Y_I=Y_P+d_P$ to obtain the following:

$$q=q_P+(Y_P+d_P)kAU. \tag{B3}$$

Further, $Y_P$ can be substituted by $q_P/[kA(1-U)]$ in (B3) and after rearranging we find that

$$q=q_P\frac{1}{(1-U)}+d_P kAU. \tag{B4}$$

Using a derived distribution approach, we relate (B1) and (B4) to find the following PDF for the total streamflow jump when $Y > d_P$

$$b''(q)=(1-U)\gamma_P \exp[-(1-U)\gamma_P(q-kAUd_P)]H(q-kAUd_P). \tag{B5}$$

**Acknowledgments**
We thank the editors and reviewers for their valuable comments, criticisms, and suggestions. The first and third authors gratefully acknowledge the financial support provided by the Pennsylvania Sea Grant. The fifth author acknowledges the financial support provided by FONDECYT (grant 1131131) and CONICYT/FONDAP (grant 15110020). The present work was partially developed within the framework of the Panta Rhei Research Initiative of the International Association of Hydrological Sciences.

## References

Abramowitz, M., and I. A. Stegun (1964), *Handbook of Mathematical Functions with Formulas, Graphs, and Mathematical Tables*, U.S. Gov. Print. Off., Washington, D. C.
Baker, D. B., R. P. Richards, T. T. Loftus, and J. W. Kramer (2004), A new flashiness index: Characteristics and applications to midwestern rivers and streams, *J. Am. Water Resour. Assoc.*, *40*(2), 503–522.
Basso, S., and G. Botter (2012), Streamflow variability and optimal capacity of run-of-river hydropower plants, *Water Resour. Res.*, *48*, W10527, doi:10.1029/2012WR012017.
Basu, N. B., et al. (2010), Nutrient loads exported from managed catchments reveal emergent biogeochemical stationarity, *Geophys. Res. Lett.*, *37*, L23404, doi:10.1029/2010GL045168.
Beighley, R. E., and G. E. Moglen (2003), Adjusting measured peak discharges from an urbanizing watershed to reflect a stationary land use signal, *Water Resour. Res.*, *39*(4), 1093, doi:10.1029/2002WR001846.
Botter, G., A. Porporato, I. Rodriguez-Iturbe, and A. Rinaldo (2007a), Basin-scale soil moisture dynamics and the probabilistic characterization of carrier hydrologic flows: Slow, leaching-prone components of the hydrologic response, *Water Resour. Res.*, *43*, W02417, doi:10.1029/2006WR005043.
Botter, G., F. Peratoner, A. Porporato, I. Rodriguez-Iturbe, and A. Rinaldo (2007b), Signatures of large-scale soil moisture dynamics on streamflow statistics across U.S. climate regimes, *Water Resour. Res.*, *43*, W11413, doi:10.1029/2007WR006162.
Botter, G., A. Porporato, E. Daly, I. Rodriguez-Iturbe, and A. Rinaldo (2007c), Probabilistic characterization of base flows in river basins: Roles of soil, vegetation, and geomorphology, *Water Resour. Res.*, *43*, W06404, doi:10.1029/2006WR005397.
Botter, G., S. Zanardo, A. Porporato, I. Rodriguez-Iturbe, and A. Rinaldo (2008), Ecohydrological model of flow duration curves and annual minima, *Water Resour. Res.*, *44*, W08418, doi:10.1029/2008WR006814.
Botter, G., S. Basso, A. Porporato, I. Rodriguez-Iturbe, and A. Rinaldo (2010), Natural streamflow regime alterations: Damming of the Piave river basin (Italy), *Water Resour. Res.*, *46*, W06522, doi:10.1029/2009WR008523.
Botter, G., S. Basso, I. Rodriguez-Iturbe, and A. Rinaldo (2013), Resilience of river flow regimes, *Proc. Natl. Acad. Sci. U. S. A.*, *110*(32), 12,925–12,930.
Braud, I., P. Breil, F. Thollet, M. Lagouy, F. Branger, C. Jacqueminet, S. Kermadi, and K. Michel (2013), Evidence of the impact of urbanization on the hydrological regime of a medium-sized periurban catchment in France, *J. Hydrol.*, *485*, 5–23.
Brun, S. E., and L. E. Band (2000), Simulating runoff behavior in an urbanizing watershed, computers, *Environ. Urban Syst.*, *24*(1), 5–22.
Bunn, S. E., and A. H. Arthington (2002), Basic principles and ecological consequences of altered flow regimes for aquatic biodiversity, *Environ. Manage. N. Y.*, *30*(4), 492–507.

Byrd, R., M. Hribar, and J. Nocedal (1999), An interior point algorithm for large-scale nonlinear programming, *SIAM J. Optim.*, *9*(4), 877–900.
Ceola, S., I. Hödl, M. Adlboller, G. Singer, E. Bertuzzo, L. Mari, G. Botter, J. Waringer, T. J. Battin, and A. Rinaldo (2013), Hydrologic variability affects invertebrate grazing on phototrophic biofilms in stream microcosms, *PLoS ONE*, *8*(4), e60629.
Claps, P., A. Giordano, and F. Laio (2005), Advances in shot noise modeling of daily streamflows, *Adv. Water Resour.*, *28*(9), 992–1000.
Clausen, B., and B. J. F. Biggs (1997), Relationships between benthic biota and hydrological indices in New Zealand streams, *Freshwater Biol.*, *38*(2), 327–342.
Coutu, S., D. Del Giudice, L. Rossi, and D. A. Barry (2012a), Modeling of facade leaching in urban catchments, *Water Resour. Res.*, *48*, W12503, doi:10.1029/2012WR012359.
Coutu, S., D. Del Giudice, L. Rossi, and D. A. Barry (2012b), Parsimonious hydrological modeling of urban sewer and river catchments, *J. Hydrol.*, *464–465*, 477–484.
Cox, D. R., and H. D. Miller (1965), *The Theory of Stochastic Processes*, Methuen & Co Ltd., London, U. K.
Daly, E., and A. Porporato (2010), Effect of different jump distributions on the dynamics of jump processes, *Phys. Rev. E*, *81*(6), 061133.
Doheny, E. J. (1999), Index of hydrologic characteristics and data resources for the Gwynn Falls Watershed, Baltimore County, and Baltimore City, Maryland, *U.S. Geol. Surv. Open File Rep. 99–213*, p. 17, Baltimore, Md.
Doyle, M. W. (2005), Incorporating hydrologic variability into nutrient spiraling, *J. Geophys. Res.*, *110*, G01003, doi:10.1029/2005JG000015.
Falkenmark, M. (2003), Freshwater as shared between society and ecosystems: From divided approaches to integrated challenges, *Philos. Trans. R. Soc. London B*, *358*(1440), 2037–2049.
Fenneman, N. M. (1938), *Physiography of Eastern United States*, 1st ed., 714 pp., McGraw-Hill, New York.
Froelich, A. J., J. T. Hack, and E. G. Otton (1980), *Geologic and Hydrologic Map Reports for Land-Use Planning in the Baltimore-Washington Urban Area*, 26 pp., U.S. Geol. Surv., Reston, Va.
Gao, Y., R. M. Vogel, C. N. Kroll, N. L. Poff, and J. D. Olden (2009), Development of representative indicators of hydrologic alteration, *J. Hydrol.*, *374*(1–2), 136–147.
Gironas, J., J. Niemann, L. Roesner, F. Rodriguez, and H. Andrieu (2009), A morpho-climatic instantaneous unit hydrograph model for urban catchments based on the kinematic wave approximation, *J. Hydrol.*, *377*(3–4), 317–334.
Grimmond, C. S. B., T. R. Oke, and D. G. Steyn (1986), Urban water balance: 1. A model for daily totals, *Water Resour. Res.*, *22*(10), 1397–1403.
Groffman, P., D. Bain, L. Band, K. Belt, G. Brush, J. Grove, R. Pouyat, I. Yesilonis, and W. Zipperer (2003), Down by the riverside: Urban riparian ecology, *Frontiers Ecol. Environ.*, *1*(6), 315–321.
Hamel, P., E. Daly, and T. D. Fletcher (2013), Source-control stormwater management for mitigating the impacts of urbanisation on baseflow: A review, *J. Hydrol.*, *485*(0), 201–211.
Hejazi, M. I., and G. E. Moglen (2007), Regression-based approach to low flow prediction in the Maryland Piedmont region under joint climate and land use change, *Hydrol. Processes*, *21*(14), 1793–1801.
Hejazi, M. I., and G. E. Moglen (2008), The effect of climate and land use change on flow duration in the Maryland Piedmont region, *Hydrol. Processes*, *22*(24), 4710–4722.
Isham, V., D. R. Cox, I. Rodríguez-Iturbe, A. Porporato, and S. Manfreda (2005), Representation of space–time variability of soil moisture, *Proc. R. Soc. A*, *461*(2064), 4035–4055.
Isik, S., L. Kalin, J. E. Schoonover, P. Srivastava, and B. Graeme Lockaby (2013), Modeling effects of changing land use/cover on daily streamflow: An artificial neural network and curve number based hybrid approach, *J. Hydrol.*, *485*(0), 103–112.
Karr, J. R. (1991), Biological integrity: A long-neglected aspect of water resource management, *Ecol. Appl.*, *1*(1), 66–84.
Klein, R. D. (1979), Urbanization and stream quality impairment, *J. Am. Water Resour. Assoc.*, *15*(4), 948–963.
Konrad, C., and D. Booth (2005), Hydrologic changes in urban streams and their ecological significance, in *Effects of Urbanization on Stream Ecosystems*, edited by L. R. Brown et al., pp. 157–177, Am. Fish. Soc., Symposium 47, Bethesda, Md.
Laio, F. (2006), A vertically extended stochastic model of soil moisture in the root zone, *Water Resour. Res.*, *42*, W02406, doi:10.1029/2005WR004502.
Laio, F., A. Porporato, L. Ridolfi, and I. Rodriguez-Iturbe (2001), Plants in water-controlled ecosystems: Active role in hydrologic processes and response to water stress: II. Probabilistic soil moisture dynamics, *Adv. Water Resour.*, *24*(7), 707–723.
Lazzaro, G., S. Basso, M. Schirmer, and G. Botter (2013), Water management strategies for run-of-river power plants: Profitability and hydrologic impact between the intake and the outflow, *Water Resour. Res.*, *49*, 8285–8298, doi:10.1002/2013WR014210.
Leopold, L. B. (1968), *Hydrology for Urban Land Planning: A Guidebook on the Hydrologic Effects of Urban Land Use*, U.S. Geol. Surv., Washington, D. C.
McCuen, R. H., and W. M. Snyder (1986), *Hydrologic Modeling: Statistical Methods and Applications*, Prentice Hall, Englewood Cliffs, N. J.
Mitchell, V. G., and C. Diaper (2006), Simulating the urban water and contaminant cycle, *Environ. Modell. Software*, *21*(1), 129–134.
Mitchell, V. G., R. G. Mein, and T. A. McMahon (2001), Modelling the urban water cycle, *Environ. Modell. Software*, *16*(7), 615–629.
Moglen, G. E., K. C. Nelson, M. A. Palmer, J. E. Pizzuto, C. E. Rogers, and M. I. Hejazi (2004), Hydro-ecologic responses to land use in small urbanizing watersheds within the Chesapeake Bay watershed, in *Ecosystems and Land Use Change*, edited by R. S. Defries, pp. 41–60, AGU, Washington, D. C.
Moody, D. W. (1986), *National Water Summary 1985: Hydrologic Events and Surface-Water Resources*, 506 pp., U.S. Geol. Surv., Washington, D. C.
Moore, A. A., and M. A. Palmer (2005), Invertebrate biodiversity in agricultural and urban headwater streams: Implications for conservation and management, *Ecol. Appl.*, *15*(4), 1169–1177.
Morgan, R. P., and S. F. Cushman (2005), Urbanization effects on stream fish assemblages in Maryland, USA, *J. North Am. Benthol. Soc.*, *24*(3), 643–655.
Nilsson, C., and B. M. Renofalt (2008), Linking flow regime and water quality in rivers: A challenge to adaptive catchment management, *Ecol. Soc.*, *13*(2), 18.
Nilsson, C., and M. Svedmark (2002), Basic principles and ecological consequences of changing water regimes: Riparian plant communities, *Environ. Manage. N. Y.*, *30*(4), 468–480.
Olden, J. D., and N. L. Poff (2003), Redundancy and the choice of hydrologic indices for characterizing streamflow regimes, *River Res. Appl.*, *19*(2), 101–121.
Paul, M., and J. Meyer (2001), Streams in the urban landscape, *Annu. Rev. Ecol. Syst.*, *32*, 333–365.
Petrucci, G., E. Rioust, J. Deroubaix, and B. Tassin (2013), Do stormwater source control policies deliver the right hydrologic outcomes?, *J. Hydrol.*, *485*, 188–200.
Pinay, G., J. C. Clement, and R. J. Naiman (2002), Basic principles and ecological consequences of changing water regimes on nitrogen cycling in fluvial systems, *Environ. Manage. N. Y.*, *30*(4), 481–491.

Poff, N. L., and J. D. Allan (1995), Functional-organization of stream fish assemblages in relation to hydrological variability, *Ecology*, *76*(2), 606–627.
Poff, N. L., and J. K. H. Zimmerman (2010), Ecological responses to altered flow regimes: A literature review to inform the science and management of environmental flows, *Freshwater Biol.*, *55*(1), 194–205.
Poff, N. L., J. D. Allan, M. B. Bain, J. R. Karr, K. L. Prestegaard, B. D. Richter, R. E. Sparks, and J. C. Stromberg (1997), The natural flow regime, *Bioscience*, *47*(11), 769–784.
Poff, N. L., B. P. Bledsoe, and C. O. Cuhaciyan (2006), Hydrologic variation with land use across the contiguous United States: Geomorphic and ecological consequences for stream ecosystems, *Geomorphology*, *79*(3–4), 264–285.
Poff, N. L., et al. (2010), The ecological limits of hydrologic alteration (ELOHA): A new framework for developing regional environmental flow standards, *Freshwater Biol.*, *55*(1), 147–170.
Porporato, A., E. Daly, and I. Rodriguez-Iturbe (2004), Soil water balance and ecosystem response to climate change, *Am. Nat.*, *164*(5), 625–632.
Power, M. E., A. Sun, G. Parker, W. E. Dietrich, and J. T. Wootton (1995), Hydraulic food-chain models, *Bioscience*, *45*(3), 159–167.
Pumo, D., L. Noto, and F. Viola (2013), Ecohydrological modelling of flow duration curve in Mediterranean river basins, *Adv. Water Resour.*, *52*(0), 314–327.
Richter, B. D., J. V. Baumgartner, J. Powell, and D. P. Braun (1996), A method for assessing hydrologic alteration within ecosystems, *Conserv. Biol.*, *10*(4), 1163–1174.
Rodriguez-Iturbe, I., A. Porporato, L. Ridolfi, V. Isham, and D. R. Coxi (1999), Probabilistic modelling of water balance at a point: The role of climate, soil and vegetation, *Proc. R. Soc. London A*, *455*(1990), 3789–3805.
Rutledge, A. T., and T. O. Mesko (1996), *Estimated Hydrologic Characteristics of Shallow Aquifer Systems in the Valley and Ridge, the Blue Ridge, and the Piedmont Physiographic Provinces Based on Analysis of Streamflow Recession and Base Flow*, 58 pp., U.S. Geol. Surv., Washington, D. C.
Shields, C. A., L. E. Band, N. Law, P. M. Groffman, S. S. Kaushal, K. Savvas, G. T. Fisher, and K. T. Belt (2008), Streamflow distribution of non-point source nitrogen export from urban-rural catchments in the Chesapeake Bay watershed, *Water Resour. Res.*, *44*, W09416, doi: 10.1029/2007WR006360.
Smakhtin, V. U. (2001), Low flow hydrology: A review, *J. Hydrol.*, *240*(3–4), 147–186.
Thompson, S. E., N. B. Basu, J. Lascurain, A. Aubeneau, and P. S. C. Rao (2011), Relative dominance of hydrologic versus biogeochemical factors on solute export across impact gradients, *Water Resour. Res.*, *47*, W00J05, doi:10.1029/2010WR009605.
Tockner, K., F. Malard, and J. Ward (2000), An extension of the flood pulse concept, *Hydrol. Processes*, *14*(16–17), 2861–2883.
Valkó, P. P., and J. Abate (2004), Comparison of sequence accelerators for the Gaver method of numerical Laplace transform inversion, *Comput. Math. Appl.*, *48*(3–4), 629–636.
Vannote, R., G. Minshall, K. Cummins, J. Sedell, and C. Cushing (1980), River continuum concept, *Can. J. Fish. Aquat. Sci.*, *37*(1), 130–137.
Verma, P., J. Yeates, and E. Daly (2011), A stochastic model describing the impact of daily rainfall depth distribution on the soil water balance, *Adv. Water Resour.*, *34*(8), 1039–1048.
Vogel, R., and N. Fennessey (1994), Flow-duration curves. I: New interpretation and confidence intervals, *J. Water Resour. Plann. Manage.*, *120*(4), 485–504.
Voinov, A., R. Costanza, L. Wainger, R. Boumans, F. Villa, T. Maxwell, and H. Voinov (1999), Patuxent landscape model: Integrated ecological economic modeling of a watershed, *Environ. Modell. Software*, *14*(5), 473–491.
Walsh, C. J., A. H. Roy, J. W. Feminella, P. D. Cottingham, P. M. Groffman, and R. P. Morgan (2005), The urban stream syndrome: current knowledge and the search for a cure, *J. North Am. Benthol. Soc.*, *24*(3), 706–723.
Walsh, C. J., T. D. Fletcher, and M. J. Burns (2012), Urban stormwater runoff: A new class of environmental flow problem, *PLoS One*, *7*(9), e45814.
Wang, D., and X. Cai (2010), Recession slope curve analysis under human interferences, *Adv. Water Resour.*, *33*(9), 1053–1061.
Zanardo, S., C. J. Harman, P. A. Troch, P. S. C. Rao, and M. Sivapalan (2012), Intra-annual rainfall variability control on interannual variability of catchment water balance: A stochastic analysis, *Water Resour. Res.*, *48*, W00J16, doi:10.1029/2010WR009869.